Behavior of Concrete-Filled Steel Tube Columns under Fire

Emad AL-Wsabi[1,*], Nabil Falah[2,*]

Abstract

This paper presents the results of a numerical study of fire resistance of concrete-filled steel tube (CFST) columns, using ABAQUS program. An analytical approach consisting of three sequential analytical steps, namely, fire analysis, heat transfer analysis, and stress analysis to predicting the behavior of CFST columns under fire loading. Those included nonlinear 3D finite element models for both heat transfer and stress analysis. The illustrative model is validated by means of comparison between the numerical output data and the experimental results available in the literature. The test is for the fire resistance of CFST column subjected to the standard ASTM fire and bearing axial compression. Hence, a good agreement had been observed between the numerical and experimental results. Therefore, the finite element models are able to predict the behavior of CFST columns under fire loading.

Keywords: Concrete-filled Steel Tube, Concrete Core, Steel Tube, Heat Flux, Fire, High Temperatures, Eurocode, Interface Element, ABAQUS, Finite Element.

1. Introduction

The CFST columns began to be used in the middle of the twentieth century. It has become widely used to construct high-rise buildings and bridges in recent years, due to the excellent structural performance, which takes advantage of the combined effect between the steel tube and concrete core that work together. The steel tube strict the concrete, leading to increase compression strength, simultaneously the concrete inside the steel tube resist the deformation and the local buckling even enabling the use of thinner cross-sections. This type of composite section provides a series of features consist of high load-bearing capacity, high earthquake resistance, attractive appearance, thin cross-section, rapid construction technology and high fire resistance without external

[1] Department of Civil Engineering, Faculty of Engineering, University of Science and Technology, Sana'a, Yemen.
[2] Department of Civil Engineering, Faculty of Engineering, Sana'a University, Sana'a, Yemen.
[*] Correspondence Authors: (emadeng2011@hotmail.com), (nabilfalah@hotmail.com)

protection. These features made The CFST columns a good alternative for designers and structural engineers [1].

The CFST columns operate efficiently because it's resistance against fire is higher than the resistance of the hollow steel columns, also it does not need fire protection for the external side in most cases. While steel tube was being exposed to the fire, the steel tube expand faster than the concrete core .Therefore, the steel tube carries a higher amount of the applied load. The heat flux is gradually transferred from the steel tube to the concrete infill, the temperature rise in steel tube is relatively slow because concrete infill absorb heat from the steel tube wall, which in turn reduces the high temperatures on the steel tube. After a certain period of fire exposure (between 30 and 20 minutes), the strength and the stiffness of steel tube start to decrease quickly due to its high temperature. Therefore, the load is gradually transported to the concrete core. At this time the steel tube works only as a protection for the concrete from direct exposure of fire and keeps it working effectively.

With the passage of time the concrete strength starts to decreases until the failure occurs, either due to global buckling or compression strength. This evolution can be seen in Figure 1 in terms of the axial displacement measured at the top end of the column with time [1].

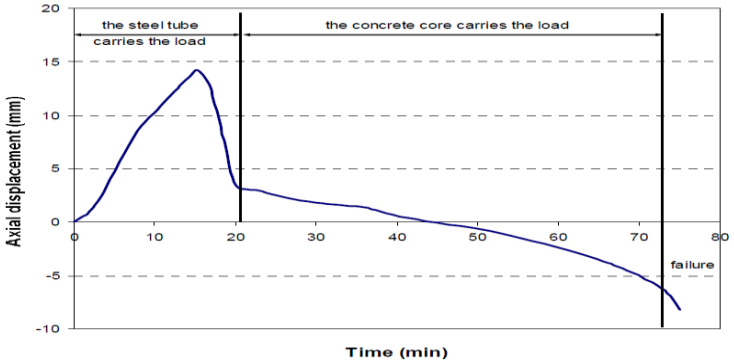

Figure(1): Typical behavior of a CFST column subjected to elevated temperatures [1].

2. Previous Experimental Study

Test of results were used to vary the numerical results according to previous experimental study conducted by experimental results because there are no laboratories specialized in this field in the our University. The test is for the fire resistance test of CFST column subjected to the standard ASTM fire and bearing axial compression as in reference [2].

The steel tubes filled with plain concrete were tested in the Institute for Research in Construction in Canada [2]. The tests were carried out as a full-scale tests on fire resistance of circular and square tubular steel columns filled with plain concrete under bearing axial

compression, apart from the specimens test C-16 was under eccentrically compression load. Test C-11 was chosen to validate the feasibility of the finite element modeling.

The fire resistance test was carried out in a furnace. The average temperature in the furnace was in accordance with ASTM-E119 standard temperature-time curve. A 219.1mm × 4.78mm steel sectioned column with 3810mm height. The columns were fixed at both ends. And its yield strength was 350MPa with 31MPa strength of the concrete at the time of the test. The aggregate type of the concrete was siliceous. The respective axial load applied at the top end of the columns was 492kN, which was about 23.1% of the axial load bearing capacity. Fire-resisting limit time was 80 minutes. The column specimen details and dimensions as presented in Figure 2- a.

Test was conducted CFST column, was carried bearing axial compression was applied approximately 45 minutes before the start of the test and shed heat. Then start shedding heat according to ASTM-E119 after the load was maintained constant throughout the test and the failure started after 80 minutes [2].

3. Numerical Analysis

There are many finite element programs (FEA) have the ability to solve a wide variety of simulations, that can be used to conduct analysis of static, dynamic, heat transfer, electrical response … etc. Also, provide both time and costs tests. In this research, The program has been selected ABAQUS/Standard 6.12, ABAQUS/Standard provides both direct and automatic user control of the time step, wide range of contact and nonlinear material options , effective for analysis the static, dynamic, thermal, and electrical response for both linear and non-linear models.

The three-dimensional numerical models were created by using ABAQUS program to simulate CFST column according to the experimental tests conducted by reference [2]. Figure 5-b, shows the column modeling in ABAQUS.

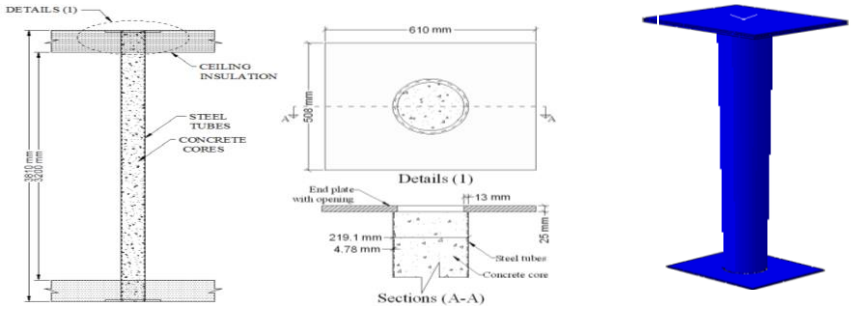

(a) **(b)**

Figure (2): Column specimen C11, a) details and dimensions b) Column CFST modeling in ABAQUS.

3.1 An Analytical Approach

It was being created the three-dimensional numerical models to simulate the experimental tests track. This track has an analytical approach consisting of three sequential analytical steps which are fire analysis, heat transfer analysis, and stress analysis.

3.1.1 Fire Analysis: There are many building codes describes an internationally agreed temperature-time curve, which is defined in the ISO 834 Standard (ISO 1980). It is characterized by a gas temperature that grows continuously along the time, but at a reduced rate. This curve has become a standard pattern which is used in the laboratories for testing the resistance of structural elements to fire, and does not represent a realistic fire. The standard ISO 834 curve, according to EC1 Part 1-2 Section 3.2.1, is calculated from the following equation [3].

$$\theta_g = 20 + 345\log_{10}(8t+1) \quad (1)$$

Where: θ_g is the gas temperature in the fire compartment [ºC], t is the time [min]

The ASTM El19-88 (Standard Methods of Fire Tests of Building Construction and Materials) is standard temperature-time curve [4]. This curve is calculated by the following approximated equation:

$$\theta_g = 20 + 750\,[1-\exp(-3.79533\sqrt{t})] + 170.1\sqrt{t} \quad (2)$$

Where: θ_g is the gas temperature in the fire compartment [ºC], t is the time [hours].

The two nominal temperature-time curves are shown in Figure 3.

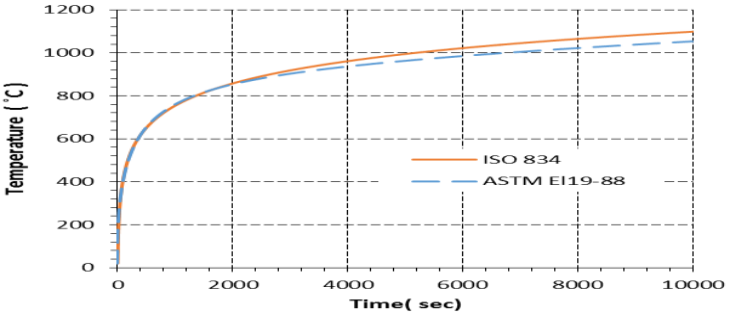

Figure (3): Two types of fire curve.

3.1.2 Heat Transfer Analysis: The heat transfer model is designed to obtain the temperature distribution at a specified time at which the fire resistance of the member wants to be verified. That the thermal properties of the materials are not independent of heat transfer, and therefore the results is highly nonlinear [1].

The heat transfer of a structural member can be divided into two parts: First part (net heat flux) the heat transfer from the fire to the exposed surface, which is a combination of the

convective and radiation heat transfer mechanisms, second part the conductive heat transfer within the structural element itself, which is evaluated through the equation for heat conduction, as presented in Figure 4.

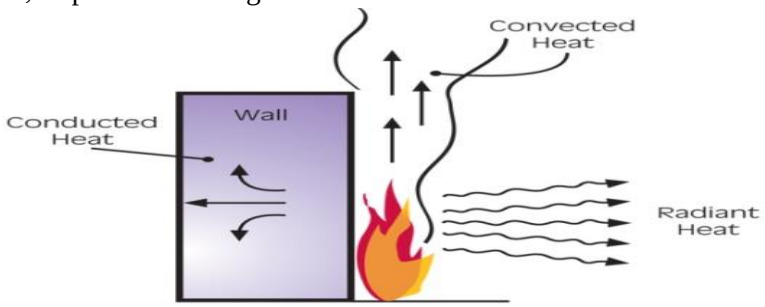

Figure (4): Heat transfer of a structural member.

On the fire exposed surfaces, the net heat flux ($\dot{h}_{net}$), according to EC1 Part 1-2 Section 3 is composite of convective heat flux ($\dot{h}_{net,c}$) and radiation heat flux ($\dot{h}_{net,r}$) as expressed as follows:

$$\dot{h}_{net} = \dot{h}_{net,c} + \dot{h}_{net,r} \ (W/m^2) \quad (3)$$

Convective heat transfer, is the transfer of heat between places by the movement of fluids, In free or natural convection, a process that is basically transfer of heat by mass transfer. The net convective heat flux component should be determined by equation:

$$\dot{h}_{net,c} = \alpha_c \ (\theta_g - \theta_m) \ (W/m^2) \quad (4)$$

where: α_c is the coefficient of heat transfer by convection equals to 25 [W/m^2K].

θ_g is the gas temperature in the vicinity of the fire exposed member [ºC].

θ_m is the surface temperature of the member [ºC].

Radiation is the transfer of energy to a body by means of the emission or absorption of electromagnetic radiation. Thermal radiation propagates through the vacuum .

The net radiation heat flux $h_{net,r}$ is determined by equation:

$$h_{net,r} = \Phi \ \varepsilon_m \ \varepsilon_f \ \sigma \ [(\theta_r + 273)^4 - (\theta_m + 273)^4] \ (W/m^2) \quad (5)$$

Where: Φ is the configuration factor equal to 1

- ε_m is the surface emissivity of the member equal to 0.7.
- εf is the emissivity of the fire, equal to 1.
- σ is the Stephan-Boltzmann constant, equal to 5.67×10-8 W/m2K4.
- θr is the effective radiation temperature of the fire environment [ºC].
- θm is the surface temperature of the member [ºC].

Conduction is the transfer of heat from one point to another due to the temperature difference. The conductive heat transfer between the contact surfaces is assumed to be defined by:

$$q = k\,(\theta_A - \theta_B) \quad (6)$$

Where q is the heat flux per unit area crossing the interface from point A on one surface to point B on the other, θ_A is the temperatures of the points on the slave surfaces [ºC], θ_B is the temperatures of the points on the master surfaces[ºC], k is the gap conductance.

3.1.3 Stress Analysis: Nonlinear stress analysis was conducted with the heat transfer analysis simultaneously to obtain the complete structural response (strain, deformation, and stress history) of CFST columns. The stress analysis was conducted using ABAQUS (2012) [5]. The structural analysis is compulsory for the determination of the fire resistance of the column takes as a starting point the previously calculated temperature distributions along with the fire exposure time. The stress and strain solution can be found for every time step, and finally the time at which the collapse of the column occurs, under a certain applied load [1].

3.2 Material Parameters

Material properties and stress-states can be affected by high temperature. In this research, the high temperature mechanical properties were used as mentioned in Eurocode.

3.2.1 Concrete at High Temperatures

3.2.1.1 Thermal Properties of Concrete at High Temperatures: It has been selected Eurocode 2 Part 1.2 (CEN 2004a) which describe in its Section 3.3 the thermal properties of concrete at high temperatures, for both concrete with siliceous and calcareous aggregates. These formulations of the concrete properties at high temperatures have been incorporated in the latest version of Eurocode 4 Part 1.2 (CEN 2005c), with subtle changes, which will be highlighted along this section. The following formulation of each of the thermal properties of concrete is according to Eurocode (2, 4).

a. Thermal elongation: The thermal elongation of concrete (Δl/l)c , according to EC2 Part 1-2 Section 3.3.1(1), may be determined from the following equations**:**

a.a. Siliceous Aggregates:

$l/l)_c$ = -1.8x10-4 + 9x10-6 θ_c + 2.3x10-11 θc3 r 20°C ≤ θ_c ≤700°C 7)

$l/l)_c = 14 \times 10^{-3}$ r 700°C ≤ θ_c ≤1200° C 8)

a.b. Calcareous Aggregates:

$l/l)_c = -1.2 \times 10^{-4} + 6 \times 10^{-6}\,\theta_c + 1.4 \times 10^{-11}\,\theta_c^3$ r 20°C ≤ θ_c ≤805°C 9)

$l/l)_c = 12 \times 10^{-3}$ r 805°C ≤ θ_c ≤1200° C .0)

Where θ_c is the concrete temperature [°C].

After using the above equations the curve between temperature and thermal elongation for concrete has been drawn, as presented in Figure 5.

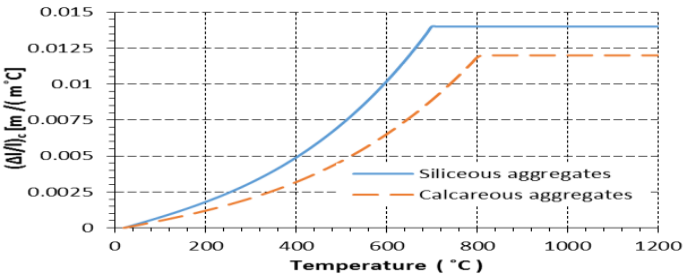

Figure (5): Thermal elongation of concrete at high temperatures [6].

In simple calculation models, according to EC4 Part 1-2 Section 3.3.2(3) [7], the relationship between the thermal elongation and concrete temperature may be considered to be linear. In this case, the elongation of concrete should be determined from the following equation:

$$(\Delta l/l)_c = 18 \times 10^{-6} (\theta_c - 20) \qquad (11)$$

Where θ_c is the concrete temperature [°C].

b. Thermal Expansion: The thermal expansion coefficient of concrete αc, is given by the following equation:

$$\alpha_C = \frac{(\Delta l/l)_c(\theta_c)}{(\theta_c - 20)} \qquad (12)$$

Where θc is the concrete temperature [°C].

After using the above equations the curve between temperature and thermal expansion for concrete has been drawn, as presented in Figure 6.

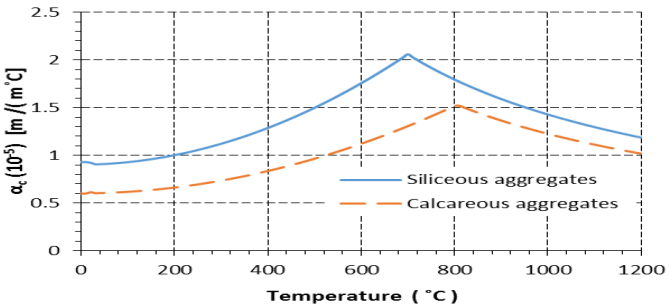

Figure (6): Thermal expansion of concrete at high temperatures [6].

c. Specific Heat: The specific heat cp (θc) of dry concrete (moisture content of= 0%), according to EC2 Part 1-2 Section 3.3.2(1), with siliceous or calcareous aggregates, may be determined from the following equations:

$(\theta_c) = 900$ [J/kg K] r $20°C \le \theta_c \le 100°C$ 3)

$(\theta_c) = 900+(\theta_c - 100)$ [J/kg K] r $100°C \le \theta_c \le 200°C$ 4)

$(\theta_c) = 1000+(\theta_c - 200) / 2$ [J/kg K] r $200°C \le \theta_c \le 400°C$ 5)

(θ_c) = 1100 [J/kg K] r 400°C ≤ θ_c ≤ 1200°C 6)

Where θ_c is the concrete temperature [°C].

If the moisture content is not considered clearly in the calculation method, the previous equations need to be amended by adding maximum value situated Cp.peak between 100 ºC and 115 ºC with linear reduction between 115°C and 200°C. This peak value with ratio moisture content is equal to:

C_p.peak = 900 J/kg K for moisture content of 0 % of concrete weight.

C_p.peak =1470 J/kg K for moisture content of 1.5 % of concrete weight.

C_p.peak = 2020 J/kg K for moisture content of 3.0 % of concrete weight.

After using the above equations the curve between temperature and specific heat for concrete has been drawn, as presented in Figure 7.

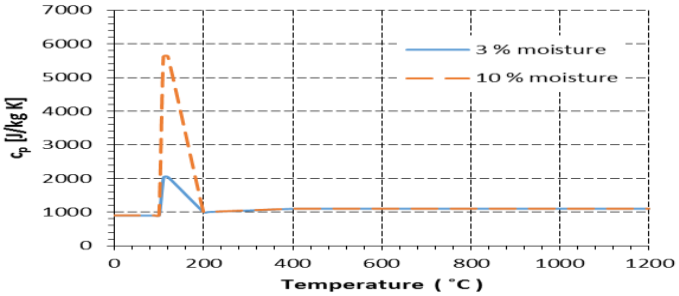

Figure (7): Specific heat of concrete at high temperatures [6].

It should be noted that, according to EC4 Part 1-2 Section 3.3.2(8), a moisture content of a 10% may be found, and in that case a value pc. Peak 5600 J/kgK should be used in hollow sections filled with concrete.

In simple calculation models, according to EC4 Part 1-2 Section 3.3.2(6) allows for the use of a constant value for the specific heat equal to 1000 J/kg K.

d. Density: The variation of density with temperature is influenced by water loss, according to EC2 Part 1-2 Section 3.3.2(3), and is defined from the following equations:

= $\rho_{(20°C)}$ r 20°C ≤ θ_c ≤ 115°C z)

= $\rho_{(20°C)}$ (1- 0.02(θ_c - 115)/85) r 115°C ≤ θ_c ≤ 200°C 8)

= $\rho_{(20°C)}$ (0.98 - 0.03(θ_c - 200)/200) r 200°C ≤ θ_c ≤ 400°C 9)

= $\rho_{(20°C)}$ (0.95 - 0.07(θ_c - 400)/800) r 400°C ≤ θ_c ≤ 1200°C 0)

where θ_c is the temperature of concrete [°C], and $\rho_{(20ºC)}$ = 2300 kg/m3.

After using the above equations the curve between temperature and density for concrete has been drawn, as presented in Figure 8.

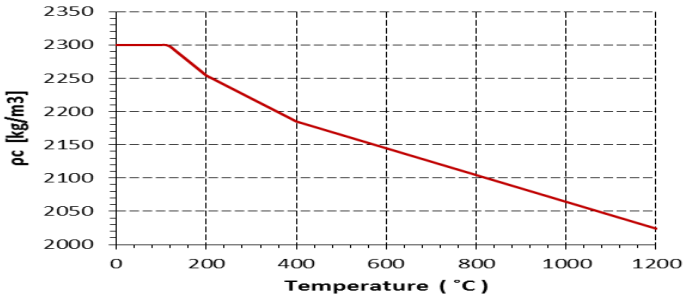

Figure(8): Density of concrete at high temperatures [6].

The concrete density with temperature, according to EC4 Part 1-2 Section 3.4(2), can also be approximated by the following expression:

$$\rho_c = 2354 - 23.47(\theta_c / 100) \quad (21)$$

where θ_c is the temperature of concrete [°C].

e. Thermal Conductivity: The thermal conductivity λc of concrete, according to EC2 Part 1-2 Section 3.3.3(2), may be determined between the lower and upper limits from the following equations:

e.a. Upper Limit

$$\lambda_c = 2-0.2451\ (\theta_c /100)+0.0107\ (\theta_c / 100)^2\ [W/mK] \quad \text{for } 20°C \le \theta_c \le 1200°C \quad (22)$$

where θ_c is the temperature of concrete [°C].

e.a. Lower Limit

$$\lambda_c = 1.36-0.136\ (\theta_c /100)+0.0057\ (\theta_c / 100)^2\ [W/m\ K] \text{ for } 20°C \le \theta_c \le 1200°C \quad (23)$$

where θ_c is the temperature of concrete [°C].

After using the above equations the curve between temperature and thermal conductivity for concrete has been drawn, as presented in Figure 9.

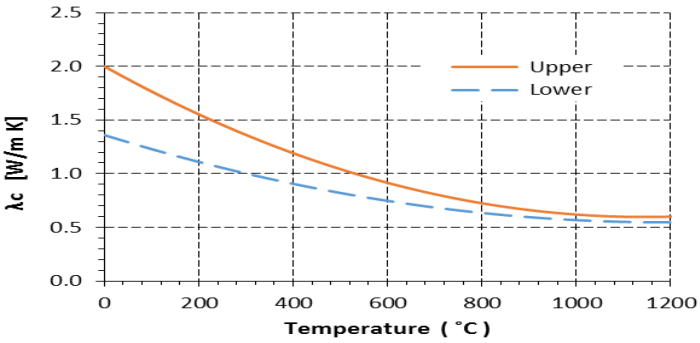

Figure (9): Thermal conductivity of concrete at high temperatures [6].

It is worth noting that, according to EC4 Part 1-2 Section 3.3.2(9) Note 2, the upper limit has been derived from tests of CFST structural elements. The use of the upper limit is recommended.

In simple calculation models, according to EC4 Part 1-2 Section 3.3.2(12), allows for the use of a constant value of 1.60 W/mK may be adopted for the thermal conductivity of concrete.

3.2.1.2 Mechanical Properties of Concrete at High Temperatures: This properties have been defined as a behavior for mechanical properties of concrete at high temperatures, according to EC2 Part 1-2 of Section 3.2.2.1, was obtained from the mechanical behavior from the stress-strain relationships as presented in Figure 10. Which can be calculated from the following equations:

Strain Range $\varepsilon_{c,\theta}$	**Stress** $\sigma_{c,\theta}$	
$\varepsilon_{c,\theta} \leq \varepsilon_{c1,\theta}$	$\sigma_{c,\theta} = \frac{3\varepsilon_{c,\theta} \cdot f_{c,\theta}}{\varepsilon_{c1,\theta}\left[2 + \left(\frac{\varepsilon_{c,\theta}}{\varepsilon_{c1,\theta}}\right)\right]}$	(24)
$\varepsilon_{c1,\theta} \leq \varepsilon_{c,\theta} \leq \varepsilon_{cu1,\theta}$	For numerical purposes, a descending branch should be adopted. Linear or non-linear models are permitted.	

Those equation models are defined by two parameters: the compressive strength ($f_{c,\theta}$) for a given temperature, the strain ($\varepsilon_{c1,\theta}$) corresponding to ($f_{c,\theta}$). The values of these parameters are obtained for each temperature through of applying the reduction factors in Table 3.1 of EC2 Part 1-2 Section 3.2.2.1 as presented in Figure 11, where the value of the ultimate strain ($\varepsilon_{cu1,\theta}$) is also included.

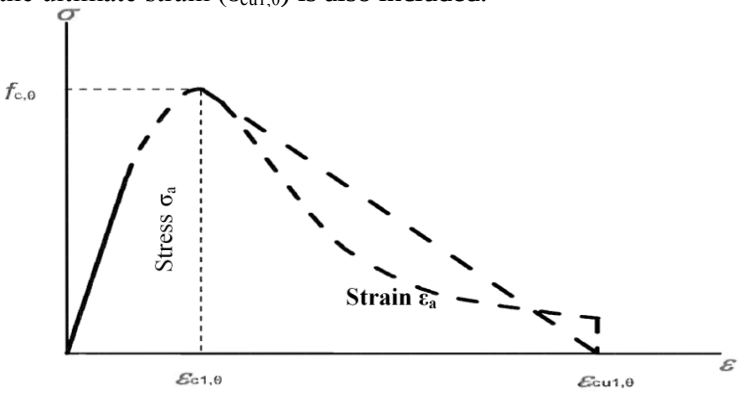

Figure (10): Mathematical model for the stress-strain relationships of concrete under compression at high temperatures [6].

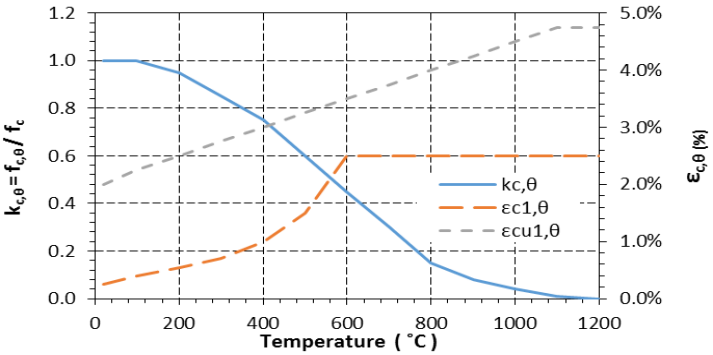

Figure (11): Reduction factors for the stress-strain relationships of concrete at high temperatures [6].

For the elastic part, the elastic modulus and Poisson's ratio were defined, the Poisson's atio was taken the value equal to 0.2. The elastic modulus of concrete was calculated at each temperature. Figure 12 shows the concrete behavior (stress-strain curve) at each temperature for a 31 MPa concrete compressive strength.

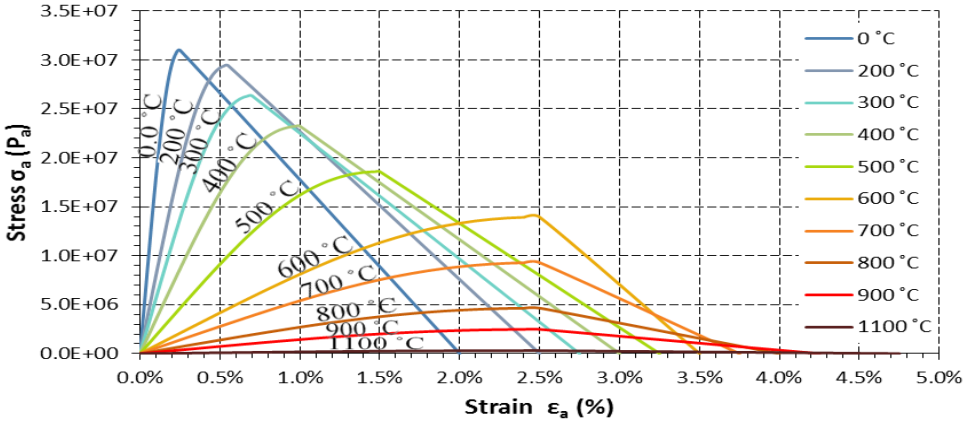

Figure(12): Stress-strain curves at high temperatures for a 31 MPa concrete [6].

3.2.2 Steel at High Temperatures

3.2.2.1 Thermal Properties of Steel at High Temperatures: This properties have been selected Eurocode 3 Part 1.2 (CEN 2005b), which describe in its Section 3.4, the thermal properties of steel at high temperatures. These formulations of the steel properties at high temperatures have been incorporated in the latest version of Eurocode 4 Part 1.2 (CEN 2005c), with subtle changes which will be addressed next. The following formulation of each of the thermal properties of steel is according to Eurocode (3,4).

a. Thermal Elongation: The thermal elongation of steel (Δl/l)a, according to EC3 Part 1-2 Section 3.4.1.1(1), was calculated from the following equations:

$l/l)_a = 1.2 \times 10^{-5}\,\theta_a + 0.4 \times 10^{-8}\,\theta_a^2 + 2.416 \times 10^{-4}$: $20°C \le \theta_a \le 750°C$ (5)

$l/l)_a = 1.1 \times 10^{-2}$: $750°C \le \theta_a \le 860°C$ (6)

$l/l)_a = 2 \times 10^{-5}\,\theta_a - 6.2 \times 10^{-3}$: $860°C \le \theta_a \le 1200°C$ (7)

Where θ_a is the steel temperature [°C].

After using the above equations the curve between temperature and thermal elongation for steel has been drawn, as presented in Figure 13.

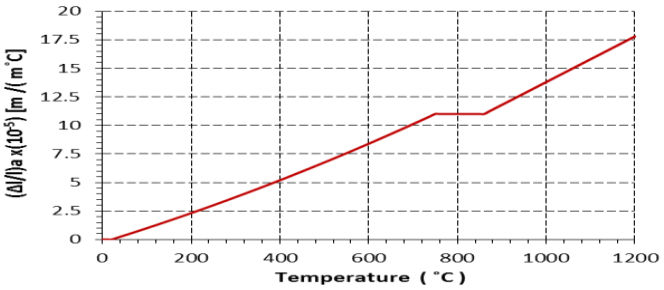

Figure(13): Thermal elongation of steel at high temperatures [8].

In simple calculation models, according to EC4 Part 1-2 Section 3.3.1(3), the relationship between the thermal elongation and steel temperature may be considered to be linear. In this case, the elongation of steel should be determined from the following equations:

$$(\Delta l/l)a = 14 \times 10\text{-}6\ (\theta_a - 20) \quad (28)$$

Where θ_a is the steel temperature [°C].

b. Thermal Expansion: The thermal expansion coefficient of steel αa, is given by the following equation:

$$\alpha_a = \frac{(\Delta l/l)_a\,(\theta_a)}{(\theta_a - 20)} \quad (29)$$

Where θ_a is the steel temperature [°C].

After using the above equations the curve between temperature and thermal expansion for steel has been drawn, as presented in Figure 14.

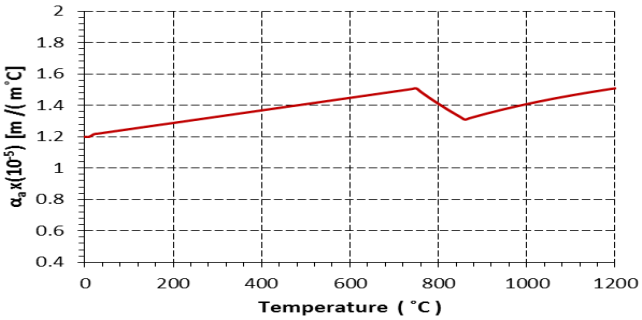

Figure (14): Thermal expansion of steel at high temperatures [8].

c. Specific Heat: The specific heat ca (θa), according to EC3 Part 1-2 Section 3.4.1.2(1), calculated by the following equations:

$c_a = 425 + 7.73 \times 10^{-1}\theta_a - 1.69 \times 10^{-3}\theta_a^2 + 2.22 \times 10^{-6}\theta_a^3$ [J/kgK] for $20°C \le \theta_a \le 600°C$ 30)

$c_a = 666 + \frac{13002}{738 - \theta_a}$ [J/kgK] for $600°C \le \theta_a \le 735\ °C$ 31)

$c_a = 545 + \frac{17820}{\theta_a - 731}$ [J/kgK] for $735°C \le \theta_a \le 900\ °C$ 32)

$c_a = 650$ [J/kgK] for $900°C \le \theta_a \le 1200°C$ 33)

Where θ_a is the steel temperature [°C].

After using the above equations the curve between temperature and specific heat for steel has been drawn, as presented in Figure 15.

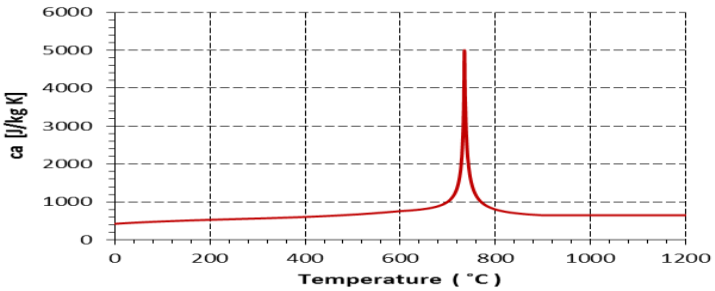

Figure (15): Specific heat of steel at high temperatures [8].

In simple calculation models, according to EC4 Part 1-2 Section 3.3.1(6), the specific heat may be considered to be independent of the steel temperature, In this case the adopting value equal to 600 J/kgK.

d. Density : The density of steel ρa, according to EC4 Part 1-2 Section 3.4 (1), shall be considered to be independent of the steel temperature. In this case, the adopting value is 7850 kg/m3.

e. Thermal Conductivity: The thermal conductivity of steel λa, according to EC3 Part 1-2 Section 3.4.1.3 (1), calculated by the following equations:

$= 54 - 3.33 \times 10^{-2}\ \theta_a$ [W/mK] r $20°C \le \theta_a \le 800\ °C$ 34)

$= 27.3$ [W/mK] r $800°C \le \theta_a \le 1200\ °C$ 35)

where θ_a is the temperature of steel [°C].

After using the above equations the curve between temperature and thermal conductivity for steel has been drawing, as presented in Figure 16.

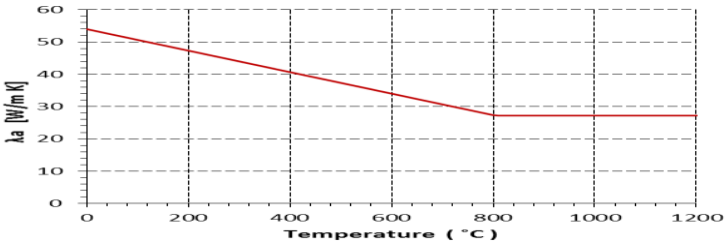

Figure(16): Thermal conductivity of steel at High temperatures [8].

In simple calculation models of the thermal conductivity, according to EC4 Part 1-2 Section 3.3.1(9), may be considered to be independent of the steel temperature, Allows the adoption of the value of 45 W/mK.

3.2.2.2 Mechanical Properties of Steel at High Temperatures: This properties have been defined as mechanical behavior of structural steel at high temperatures, according to EC3 Part 1-2 Section 3.2.1(1,2), the general stress-strain curve in Figure 17 can be used to illustrate the resistances to tension or compression. Which can be obtained from the following equations:

Strain Range ε	Stress $\sigma_{c,\theta}$	Tangent modulus	
$\varepsilon \le \varepsilon_{p,\theta}$	$\varepsilon E_{a,\theta}$	$E_{a,\theta}$	(36)
$\varepsilon_{p,\theta} < \varepsilon < \varepsilon_{y,\theta}$	$f_{p,\theta} - c + (b/a)\left[a^2 - (\varepsilon_{y,\theta} - \varepsilon)^2\right]^{0.5}$	$\frac{b(\varepsilon_{y,\theta} - \varepsilon)}{a\left[a^2 - (\varepsilon_{y,\theta} - \varepsilon)^2\right]^{0.5}}$	(37)
$\varepsilon_{y,\theta} \le \varepsilon \le \varepsilon_{t,\theta}$	$f_{y,\theta}$	0	(38)
$\varepsilon_{t,\theta} < \varepsilon < \varepsilon_{u,\theta}$	$f_{y,\theta}\left[1 - (\varepsilon - \varepsilon_{t,\theta})/(\varepsilon_{u,\theta} - \varepsilon_{t,\theta})\right]$	-	(39)
$\varepsilon = \varepsilon_{u,\theta}$	0.00	-	(40)
Parameters	$\varepsilon_{p,\theta} = f_{p,\theta} / E_{a,\theta}$ $\varepsilon_{y,\theta} = 0.02$ $\varepsilon_{t,\theta} = 0.15$ $\varepsilon_{u,\theta} = 0.2$		
Functions	$a^2 = (\varepsilon_{y,\theta} - \varepsilon_{p,\theta})(\varepsilon_{y,\theta} - \varepsilon_{p,\theta} + c / E_{a,\theta})$ $b^2 = c(\varepsilon_{y,\theta} - \varepsilon_{p,\theta}) E_{a,\theta} + c^2$ $c = \frac{(f_{y,\theta} - f_{p,\theta})^2}{(\varepsilon_{y,\theta} - \varepsilon_{p,\theta})E_{a,\theta} - 2(f_{y,\theta} - f_{p,\theta})}$		

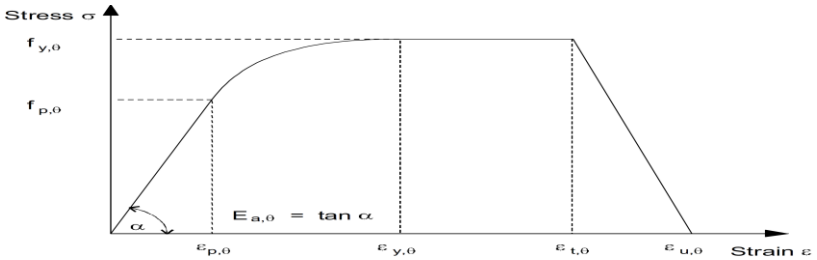

Figure (17): Stress-strain relationship for structural steel at high temperatures [8].

where:

$f_{y,\theta}$ effective yield strength.

$f_{p,\theta}$ proportional limit;

$E_{a,\theta}$ slope of the linear elastic range.

$\varepsilon_{p,\theta}$ strain at the proportional limit.

$\varepsilon_{y,\theta}$ yield strain.

$\varepsilon_{t,\theta}$ limiting strain for yield strength.

$\varepsilon_{u,\theta}$ ultimate strain.

Table 3.1 in EC3 Part 1-2 Section 3.2.1 gives the reduction factors for the parameters f_y, f_p and E_a for a certain temperature. The variation of these reduction factors with temperature is illustrated in Figure 18.

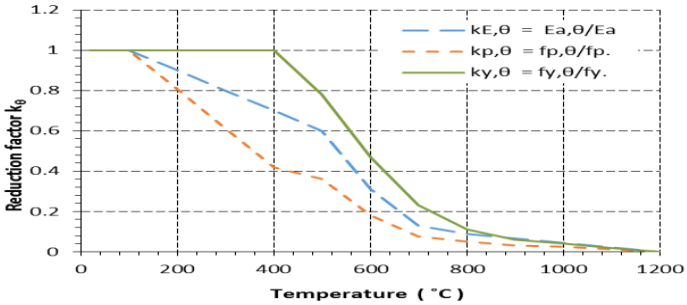

Figure 18: Reduction factors for the stress-strain relationships of structural steel at high temperatures [8].

For the elastic part, the elastic modulus and Poisson's ratio were defined, the Poisson's ratio was taken equal to 0.3, The elastic modulus of steel at high temperatures were obtained from the Table 3.1 in EC3 Part 1-2 Section 3.2.1.

Figure 19 shows the steel behavior (stress-strain curve) at each temperature for tensile strength of 350 MPa.

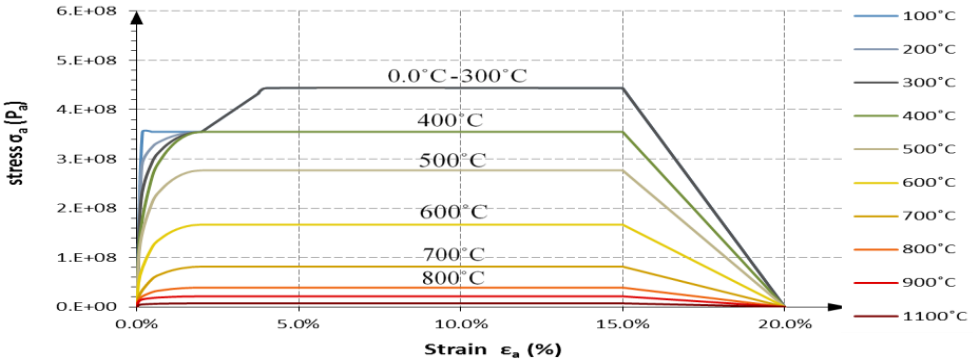

Figure (19): Stress-strain curves at elevated temperatures for a350 MPa steel [8].

3.3 Element Types

ABAQUS element library includes many elements, the names of the elements are defined in set of symbols, and each symbol has a specific function. Therefore, names of the elements differ by the change of symbols. Figure 20 describes the symbols in the elements used in this research.

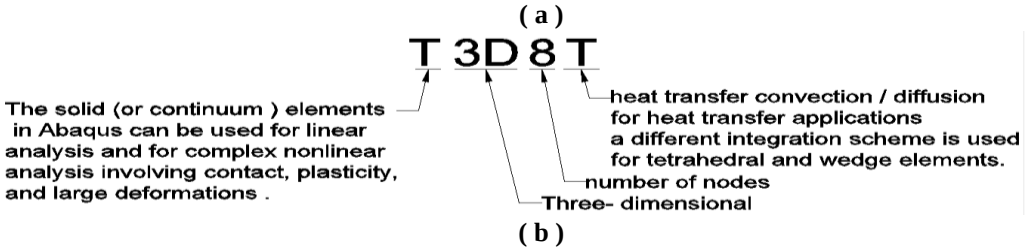

Figure (20): Description naming elements in the program ABAQUS (a) Solid elements (b)Truss elements.

For this study, three-dimensional solid elements (C3D8T) were used to model the concrete slabs, steel tubes, concrete cores, beams, bolts and channel's flanges. Three-dimensional solid elements (C3D6T) were used to model the end plate for beam and channel's web, and also three-dimensional truss elements (T3D2T) were used to model the rebar reinforcement. Figure 21 shows how the different parts and regions of the model were meshed.

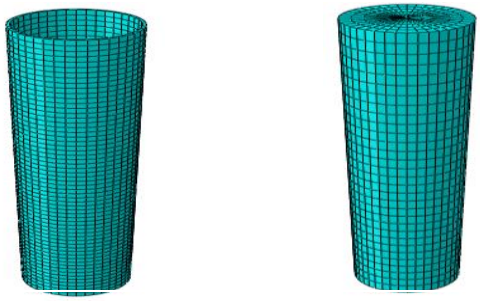

a) Steel Tubes b) Concrete Core

Figure(21): Meshing of the different parts and regions of the model

3.4 Contact Constraints & Interactions

ABAQUS provides several constraint and interactions formulations. Each contact (constraint and interactions) contains so many types. In this section, only the type that was used in this research will be illustrated.

Contact interactions on three main factors is based on a choice of a tracking approach, a contact discretization, and assignment of "master" and "slave" roles to the contact surfaces [9]. In this research, the contact interactions was used with a choice of main factors 'Small sliding' and 'surface to surface' at contact pairs simulations, as recommended by ABAQUS manual. They were used to simulate the contact interactions between Steel Tubes – Concrete Cores.

3.5 Contact Properties

Contact has a lot of properties, the mechanical and thermal properties of this contact were chosen in this research and will be explained as follow:

3.5.1 Mechanical Contact Properties: The mechanical interaction between the parts of contact surfaces was modeled using two factors: The first factor is normal behavior employed as hard contact formulation, the hard contact relationship with contact pressure can be transmitted between contact surfaces, no penetration is allowed of the slave surface into the master surface at the constraint locations which allows any pressure value transfer when the surfaces are in contact [9]. The second factor is tangential behavior that include a friction model as part of a surface, the Coulomb friction model was used with a constant friction coefficient of 0.3 [1,10].

3.5.2 Thermal contact properties: In the numerical model thermal interaction at the surfaces of the parts, where they show thermal resistance at the boundary between the parts are taken into account.

ABAQUS allows heat flow across an interface via conduction or radiation. Generally, both modes of heat transfer are present to some degree. As the results of an analysis sensitivity, a constant value of 200 W/m2K was taken for the gap conductance at the boundary between the steel tube and the concrete core [1].

4. Validation of the Model

ABAQUS program used to create a finite element models. This section will assess the accuracy of the model by comparison between the results from finite element analysis and those from fire tests conducted in the laboratories.

4.1 Test of Concrete-Filled Steel Tube Columns

The three-dimensional numerical model was developed by ABAQUS. This test was on the first stage validated by comparing its results with experimental fire resistance tests of CFST column from the literature. The column specimen used in this validation stage was tested at the National Research Council of Canada. The characteristics of the column were the same as in [2].

Figure 22 shows the results of the numerical simulations of ABAQUS program, where the temperature field along the column and its deformed shape after failure can be seen. Both the numerical and the experimental tests are shown in Figure 22.

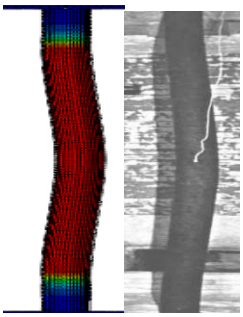

Figure (22): Deformed shapes after exposure to standard fire, for column C-11compared with [2]).

Before showing the results of CFST columns, the effect of meshing size on the results of the column in terms of heat transfer and vertical displacement is studied to guarantee the accuracy of the results. Therefore, three different meshing schemes were defined to model CFST column which are as follows:

Mesh one: The column is divided into 64 segments along the axis direction. The cross section is divided into 28 steel and 140 concrete elements, as shown in Figure 23 (a).

Mesh two: The column is divided into 90 segments along the axis direction. The cross section is divided into 40 steel and 200 concrete elements, as shown in Figure 23 (b).

Mesh three: The column is divided into 120 segments along the axis direction. The cross section is divided into 60 steel and 300 concrete elements, as shown in Figure 23 (c).

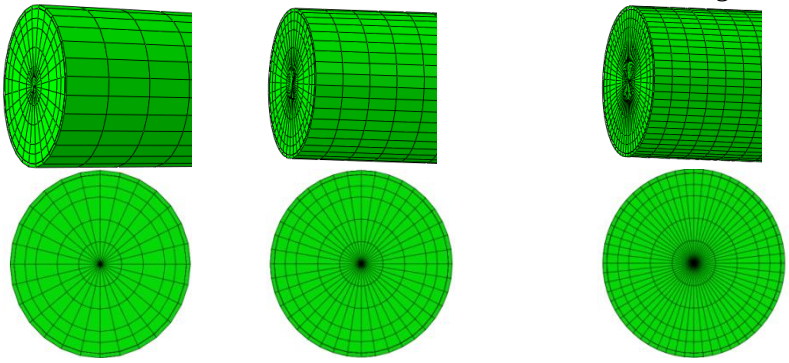

a) Mesh one b) Mesh two c) Mesh three

Figure (23): Finite element model of CFST column (a) Mesh one (b) Mesh two (c) Mesh three.

The comparisons between the temperature curves and vertical displacements from the three meshes are as shown in Figure 24, results also show the comparison between the temperature-time curves and the vertical displacements-time curves which show predicted behavior.

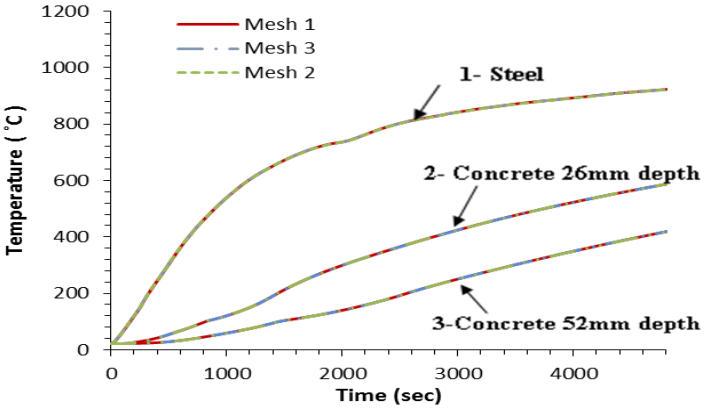

a) Temperature field

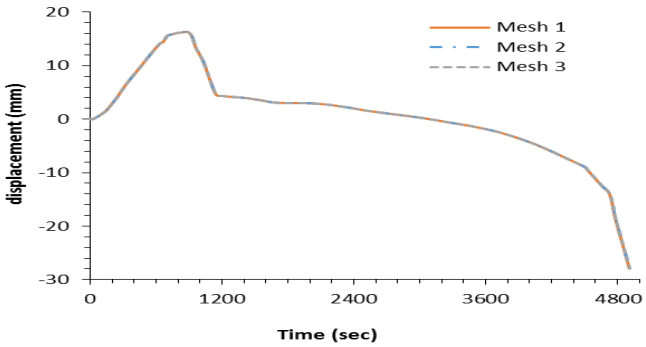

b) Vertical head displacement

Figure (24): Temperature field and Vertical head displacement using different meshes.

4.1.1 Thermal Response : The first validation step in the column test includes comparing the evolution of temperature along the fire exposure time in the numerical simulations with the temperatures of the test at those sectional points in the experimental study. The comparison shows the good agreement between numerical and experimental temperatures as in Figure 25 for the test C11 specimen.

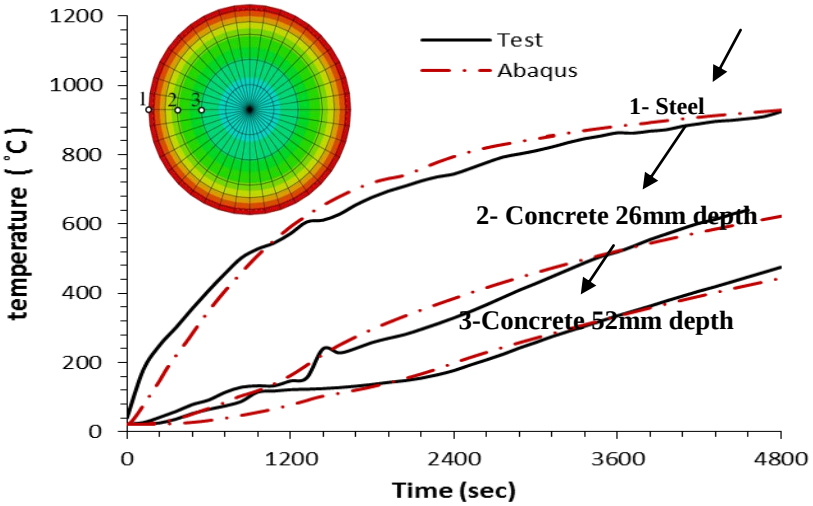

Figure (25): Comparison between numerical and experimental temperatures for column C11.

4.1.2 Mechanical Response: The second validation step in the column test includes comparing the axial displacement at the top of the column versus the fire exposure time that registered during the simulation. The comparison shows a good agreement between numerical and experimental displacement as in Figure 26 for the test C11 specimen.

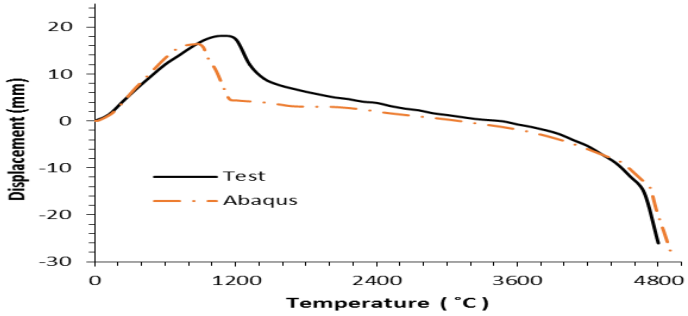

Figure (26): Comparison of numerical and experimental axial displacement.

5. Summary and Conclusions

This paper presents numerical study of the CFST column fire tests. The test is the fire behavior for axially loaded CFST column of circular cross-section that was investigated through numerical modeling. The accuracy of the numerical model was verified by means of test results which is available in the literature, showing that it can provide a realistic representation of the fire response of normal strength CFST columns.

Some conclusions can be depicted as follow:

1- A good agreement was observed between the numerical and experimental results. Thus, the finite element model is capable of predicting the fire response of normal strength CFST columns.

2- It turned out in the verification process that, the mesh size for the fire response of normal strength CFST columns has little effect.

3- Eurocode gave good results of the fire resistance of CFST columns as compared with experimental fire tests results.

6. References

[1] Capilla, A. (2012) Numerical Analysis of the Fire Resistance Circular and Elliptical Slender Concrete Filled Tubular Columns, Universitat Politècnica De València.

[2] Lie, T. and Chabot, M. (1992) 'Experimental Studies on the Fire Resistance of Hollow Steel Columns Filled With Plain Concrete, National Research Council Canada, Internal Report No. 611.

[3] Eurocode 1 (EC1), (2002) Actions on Structures, Part 1.2: General Actions - Actions on Structures Exposed to Fire. Brussels, Belgium: Comité Européen De Normalisation.

[4] American Society for Testing and Materials (ASTM), (1990) 'PStandard Methods of Fire Test of Building Construction and Materials, Philadelphia.

[5] Varma, A., Srisa-Ard, J. and Hong, S. (2004) 'Analytical Investigations of the Fire Behavior of Concrete Filled Steel Tube (CFT) Columns', ASCE, Journal of Structure Engineering, ISSN 1793-6764.

[6] Eurocode 2 (EC2), (2004) Design of Concrete Structures, Part 1.2: General Rules Structural Fire Design, Brussels, Belgium: Comité Européen De Normalisation.

[7] Eurocode 4 (EC4), (2005) Design of Composite Steel and Concrete Structures, Part 1.2: General Rules - Structural Fire Design, Brussels, Belgium: Comité Européen De Normalisation.

[8] Eurocode 3 (EC3), (2005) Design of Steel Structures, Part 1.2: General Rules Structural Fire Design, Brussels, Belgium: Comité Européen De Normalisation.

[9] ABAQUS (2012) ABAQUS/Standard Version 6.12 User's Manual: Volumes I-III.

[10] Iqbal, N. (2013) Restrained Behaviour of Beams in a Steel Frame Exposed to Fire, Luleå University of Technology.